rev. 10/96

HIGH ENERGY RESOLUTION INELASTIC X-RAY SCATTERING AT THE SRI-CAT*

A. T. Macrander

Experimental Facilities Division
Advanced Photon Source, Argonne National Laboratory
Argonne, IL 60439

ANL/XFD/VU--91198
CONF-9605201--5-Vugraphs

August 1996

To be published in the Proceedings of the workshop on "Atomic Physics with Hard X-rays from High Brilliance Synchrotron Light Sources," Argonne, IL, May 20-21, 1996.

*This work is supported by the U.S. Department of Energy, Basic Energy Sciences-Materials Sciences, under contract #W-31-109-ENG-38.

DISCLAIMER

HIGH ENERGY RESOLUTION INELASTIC X-RAY SCATTERING AT THE SRI-CAT

A.T. MACRANDER
ADVANCED PHOTON SOURCE

OUTLINE:

- station details
- science addressable by IXS
- 10 milli-eV resolution spectrometer
- 200 milli-eV resolution spectrometer
- IXS from electronic excitations in TiC and Ti

Acknowledgements:

Co-workers: V. Kushnir, M. Schwoerer-Bohning, Dohn Arms, P. Abbamonte

Collaborators: R. Blasdell, P. Montano, C. Kao, D. Price, B. Cooper

Management: D. Mills, G. Shenoy, D. Moncton

3 ID-C Inelastic Scattering Station

Scientists in Charge

Albert T. Macrander,
Tel (708) 252-5672, FAX (708) 252-0161, atm@aps.anl.gov
Vladimir I. Kushnir
Tel (708) 252-0162, FAX (708) 252-0161, kushnir@aps.anl.gov
Klaus Quast
Tel (708) 252-0165, FAX (708) 252-0161, quast@aps.anl.gov

Scientific Applications

Inelastic scattering to measure $S(\mathbf{q},\omega)$ and elastic scattering to measure $S(\mathbf{q})$ with narrow bandpass.

Energy resolution: meV to eV
Momentum resolution: < 0.35 Å^{-1}

Source Characteristics

Period	2.7	cm
K_{max} (@ 10.5 mm gap)	1.69	
Energy range	7-30	keV
Normal incidence peak power density	232	W/mm^2
Maximum power on crystal (@ 10.5 mm gap)	3.4	kW

Optics

Focussing type -	Double groove horizontal & vertical focusing, and collimating mirror	at 34.5 m
Monochromator	Liquid Gallium cooled, double crystal	at 29 m
Experiment	Station	at 52 m
Beam size at sample	1.3 x 3.0 (unfocussed)	mm^2
Resolution	10^{-7} - 10^{-4}	(ΔE/E)
Flux at sample	10^{10} - 10^{14}	Photons /(s-eV)

Detectors

CdZnTe p-i-n detector, Si avalanche photodiodes detectors, Si p-i-n detector

Special Equipment

High energy resolution monochromators , diced and undiced spherical analyzers, spectrometer with 3 m long two-theta arm.

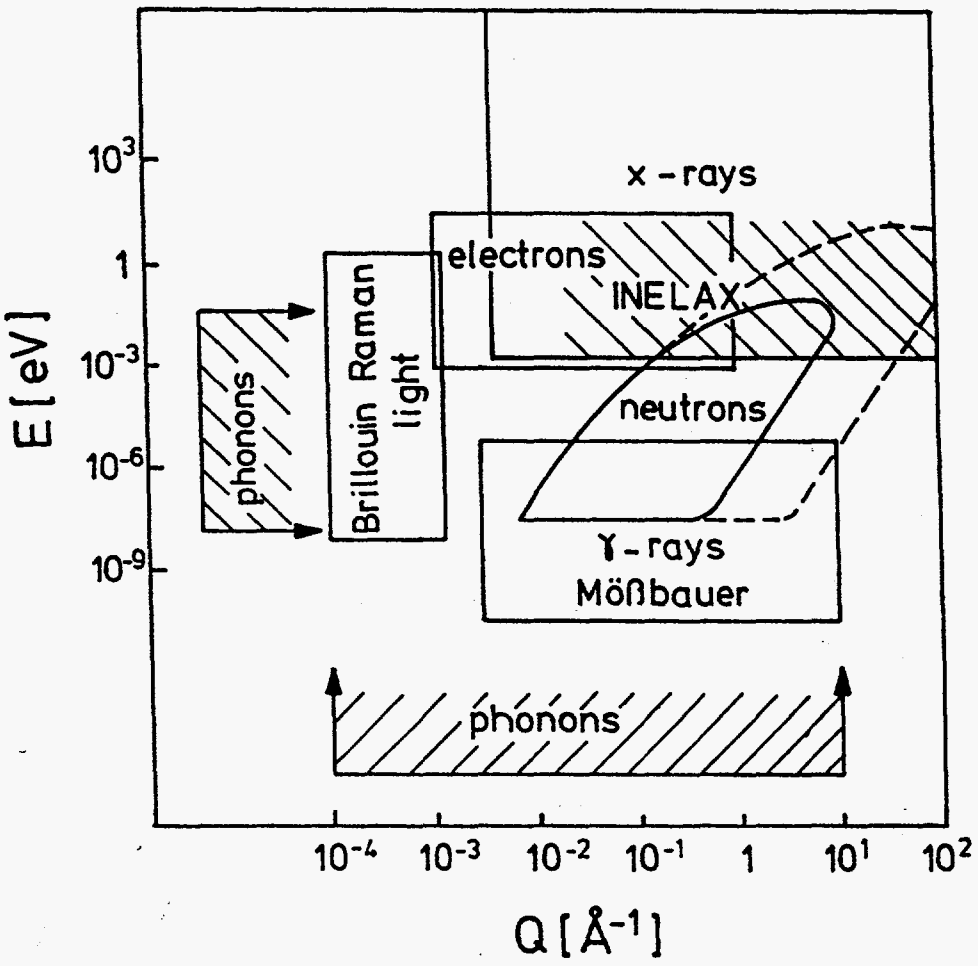

Fig. 1.1. Accessible ranges in the energy-momentum transfer space for the different probe of inelastic scattering

E. Burkel, "Inelastic Scattering of X-rays with Very High Energy Resolution", Volume 125 of *Springer Tracts in Modern Physics*, ed. G. Hohler and E.A. Niekisch, Springer-Verlag, 1991.

$S(q,\omega)$ as a function of temperature and pressure

1) **phonons:**

for q,ω not accessible with neutron scattering

e.g., fullerenes- undoped and doped, ^3He

At 13.84 keV: 10^{10} photons/sec on sample in a bandwidth of 6 meV focused to 1 mm x 1 mm

2) **elementary electronic excitations:**

plasmons
interband transitions
zone boundary collective excitations
off-diagonal terms in $\varepsilon(q,\omega)$
nonresonant Raman scattering
(resonant Raman scattering)

e.g., tests of theory that go beyond RPA in high Z materials, metal-insulator transitions, strict tests of band structure calculations.

At 7.59 keV: 10^{12} photons/sec on sample in a bandwidth of 0.1 eV focussed to 1 mm x 1 mm

3) **S(q) measurements:**

structure factor measurements with very narrow bandwidth

e.g., solid helium

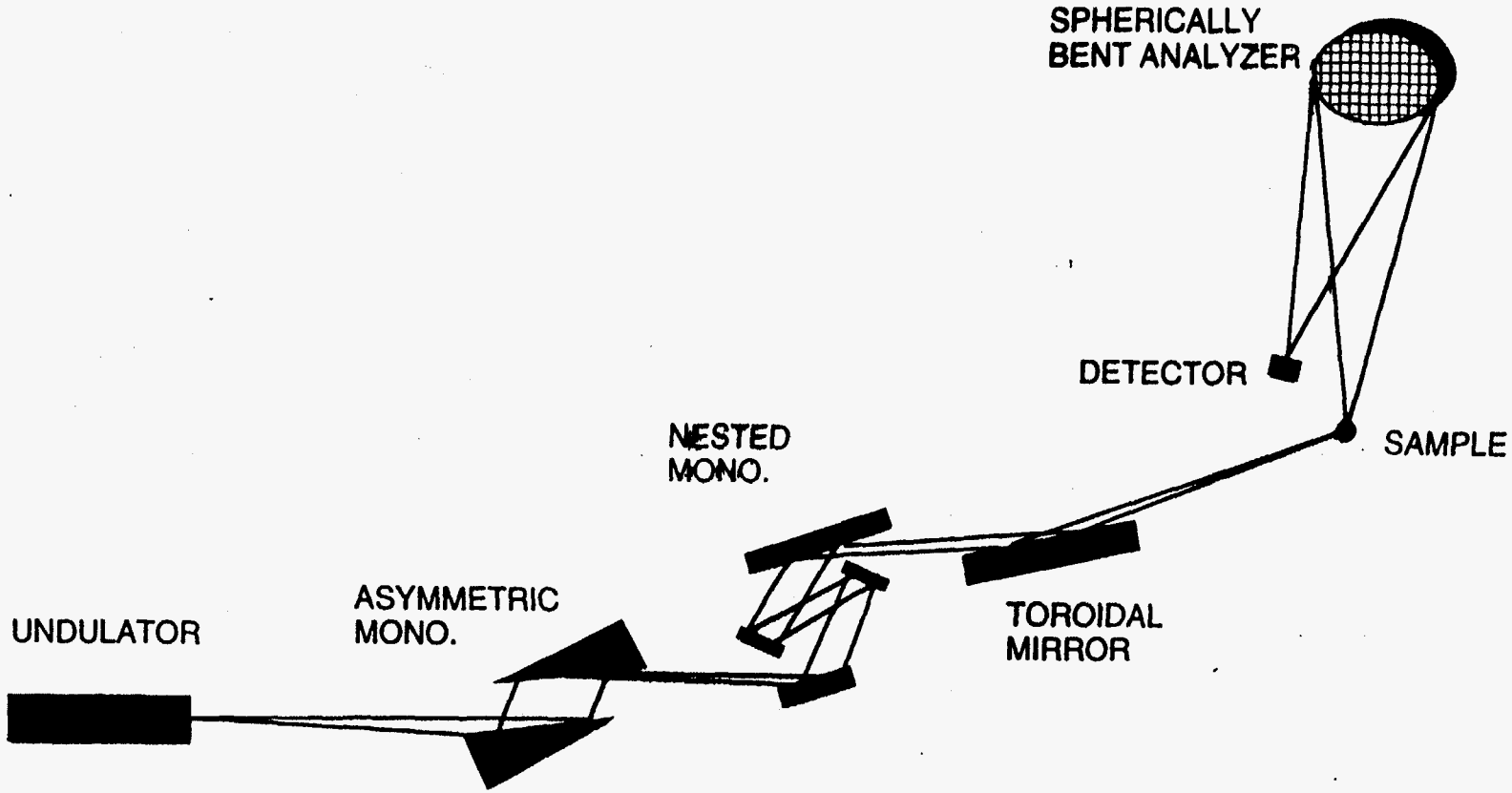

MILLI ELECTRON VOLT RESOLUTION INELASTIC SCATTERING SCHEMA

NESTED (422) X (884) MONOCHROMATOR FOR 13.84 keV

Bandpass = 5 meV

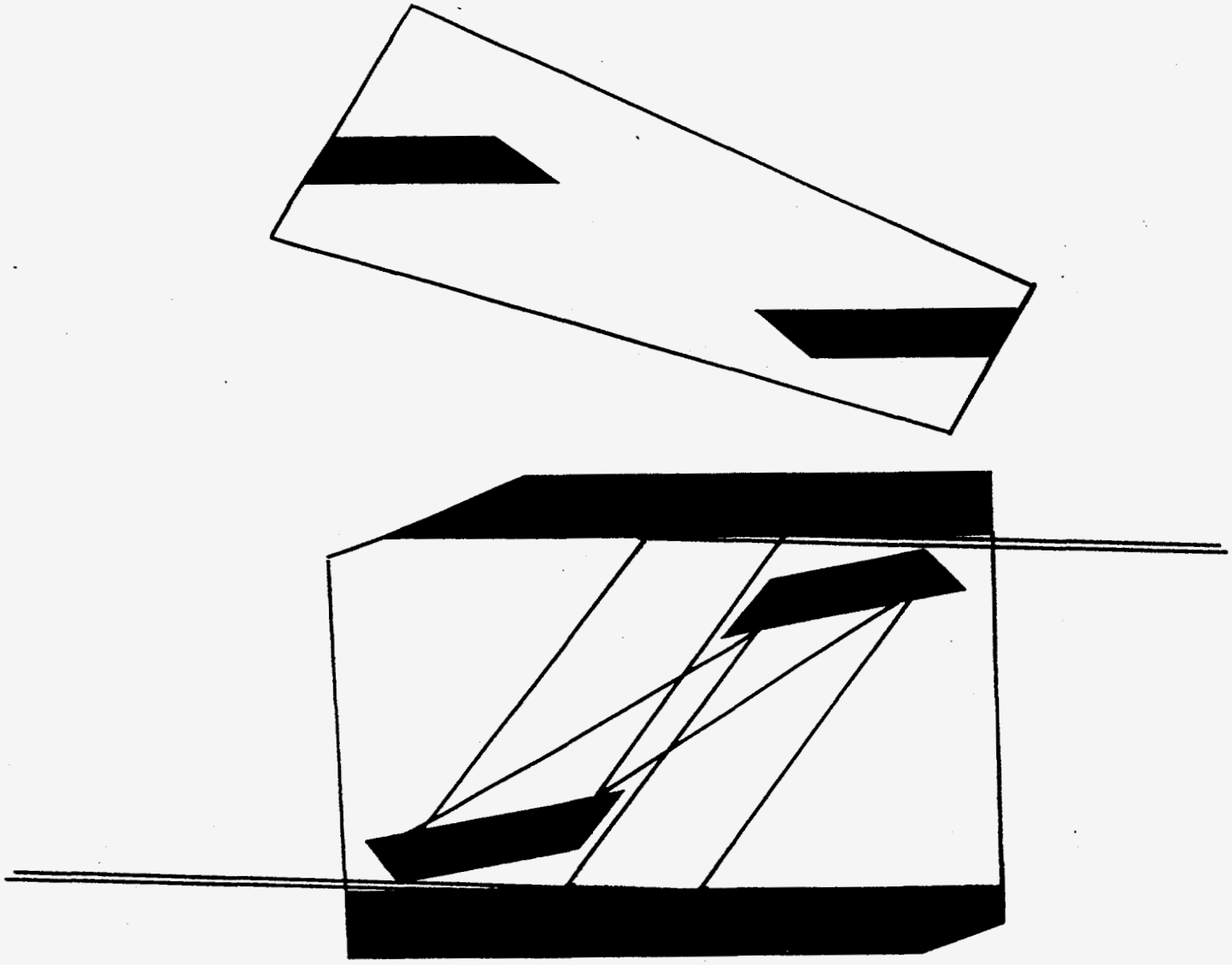

(422) x (884) HIGH RESOLUTION MONOCHROMATOR FOR 13.84 keV

Outer crystal:

Bragg reflection:	(422)
Bragg angle:	23.8 °
Darwin width:	6.4 microrad
Asymmetry angle:	21.5°
Angle of incidence:	2.3°
Dynamical b factor:	-17.5
Divergence accepted:	26.72 microrad
Divergence outgoing:	1.53 microrad
Ideal Flux ratio:	4.7

Inner crystal:

Bragg reflection:	(884)
Bragg angle:	81.8°
Darwin width:	3.7 microrad
Asymmetry angle:	60°
Angle of incidence:	21.8 °
Dynamical b factor:	-1.7
Divergence accepted:	2.8 microrad
Divergence outgoing:	4.8 microrad

Overall resolution calculated :	5.0 meV
Tuning range:	100 meV (beam walks off (884) face)
Overall ideal flux ratio:	2440

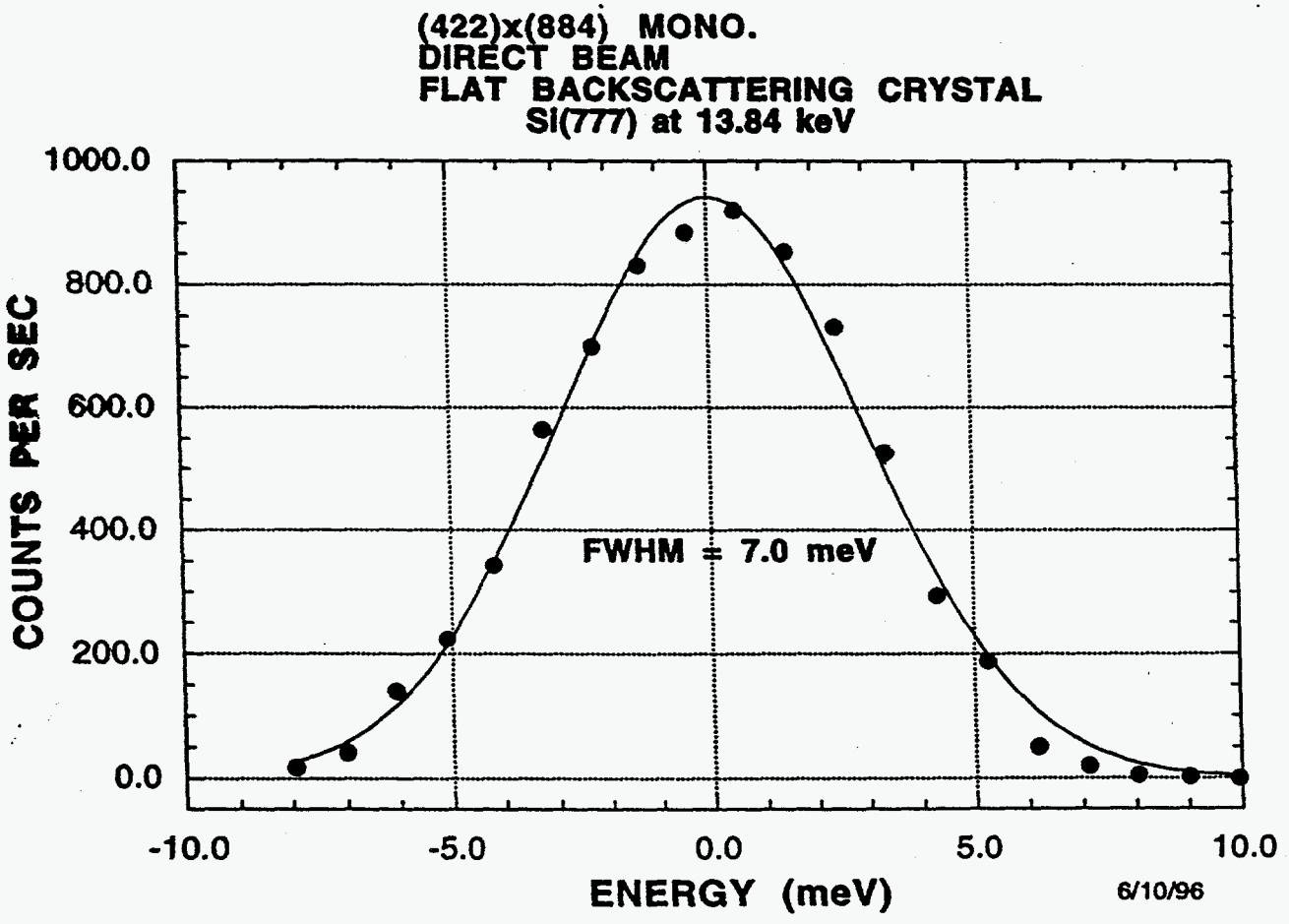
(422)x(884) MONO.
DIRECT BEAM
FLAT BACKSCATTERING CRYSTAL
Si(777) at 13.84 keV
1000.0
800.0
600.0
400.0
200.0
0.0
COUNTS PER SEC
FWHM = 7.0 meV
-10.0
-5.0
0.0
5.0
10.0
ENERGY (meV)
6/10/96

J.B. Hastings, D.E. Moncton, and Y. Fujii,
High Energy Excitations in Condensed Matter, Los Alamos, 1984.

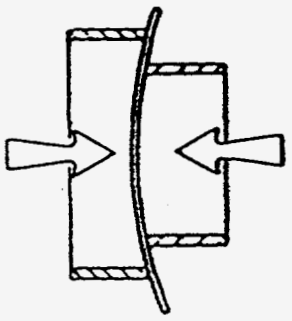

(p)

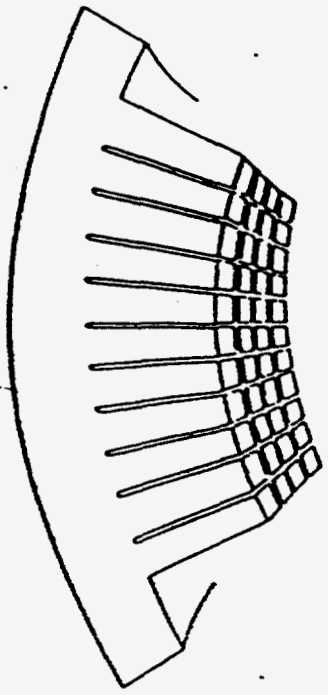

(c)

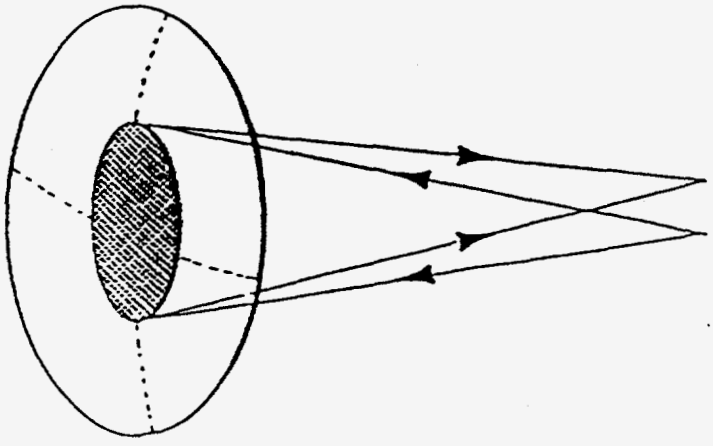

(a)

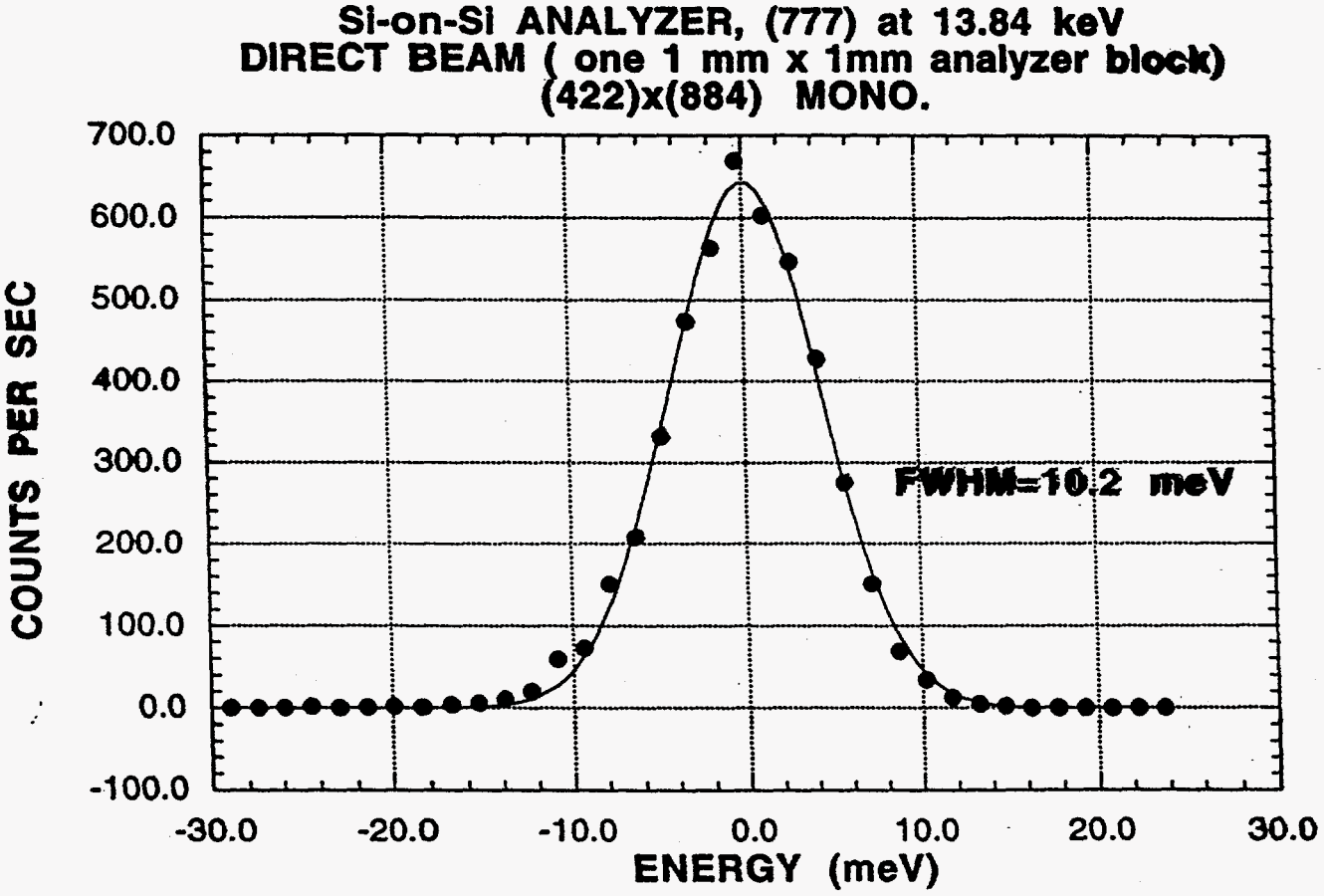
Si-on-Si ANALYZER, (777) at 13.84 keV
DIRECT BEAM (one 1 mm x 1mm analyzer block)
(422)x(884) MONO.
COUNTS PER SEC
700.0
600.0
500.0
400.0
300.0
200.0
100.0
0.0
-100.0
FWHM=10.2 meV
-30.0
-20.0
-10.0
0.0
10.0
20.0
30.0
ENERGY (meV)

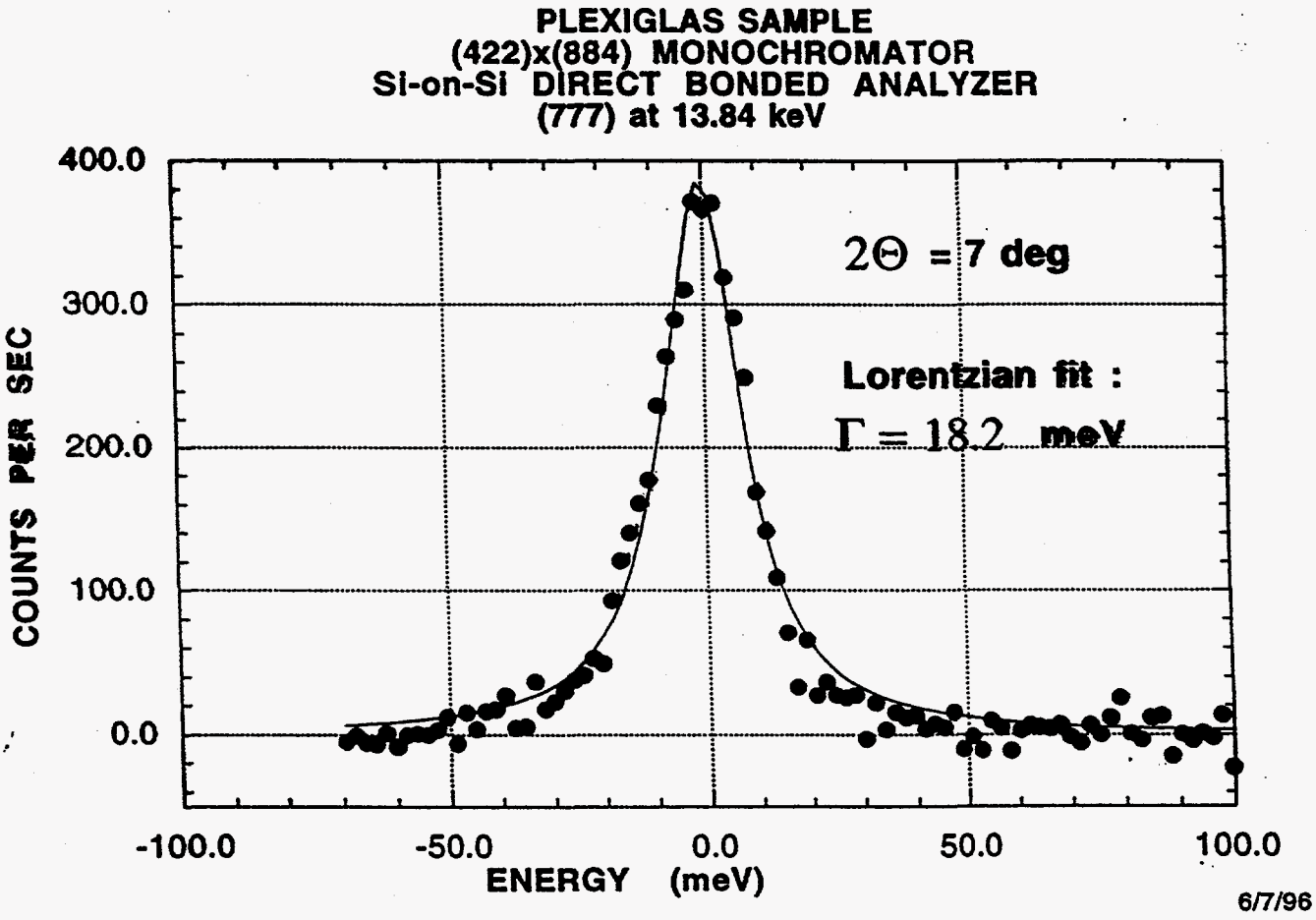
PLEXIGLAS SAMPLE
(422)x(884) MONOCHROMATOR
Si-on-Si DIRECT BONDED ANALYZER
(777) at 13.84 keV
400.0
300.0
200.0
100.0
0.0
COUNTS PER SEC
2Θ = 7 deg
Lorentzian fit :
Γ = 18.2 meV
-100.0
-50.0
0.0
50.0
100.0
ENERGY (meV)
6/7/96

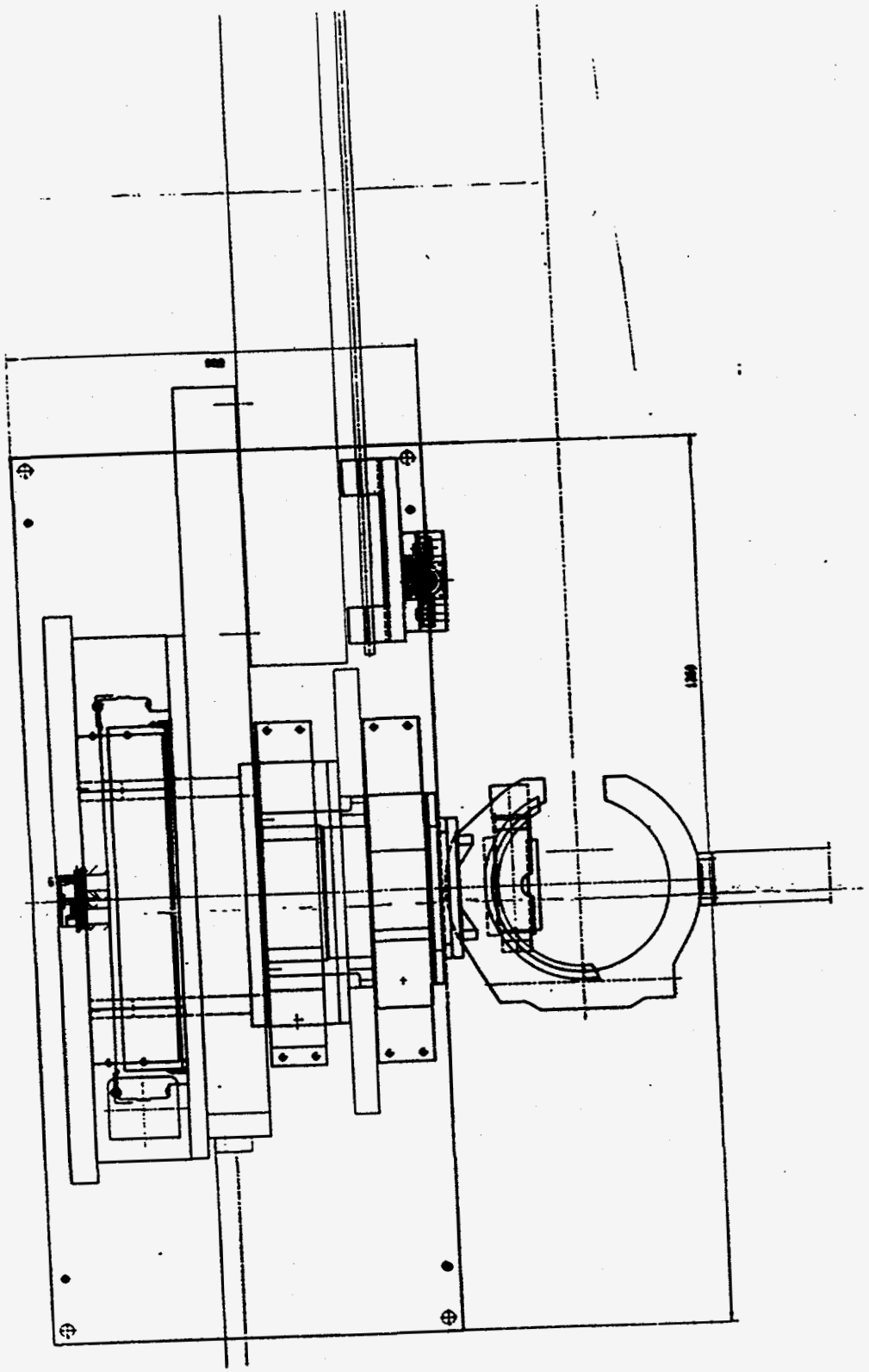

SPECIFICATIONS

SHIELDING REQUIREMENTS:
BACK WALL 1/2" THK LEAD
SIDE WALLS 3/8" THK LEAD
ROOF 1/4" THK LEAD

CONSTRUCTION: MODULAR

STRUCTURE: SELF-SUPPORTED
ROOF RATED: 40 LBS LIVE WEIGHT/SQ FT
100 LBS DEAD WEIGHT/SQ FT

OVERALL DIMS:
3.5M WIDE X 7.8M LONG X 5.5M HIGH [11.5' X 24.0' X 18.0']
CLEAR HEIGHT INSIDE: 5.0M [16']
DOOR OPENING: 2.4M HIGH X 1.0M WIDE [8' X 3.3']

SLIDING DOORS:
ONE MANUAL, FIXED BY LATCH
ONE PNEUMATIC WITH MANUAL OVERRIDE

SIDE PANEL: 1.0M WIDE X 5.5M HIGH [3.3' X 18.0']
SANDWICH CONSTRUCTION: STEEL 3mm [1/8" (11Ga.)] - LEAD 10mm[3/8"] - STEEL 6mm[1/4"]
STRUCTURE: 3" X 3" X 1/4" STEEL ANGLE, ALL AROUND
WEIGHT:3867LB

BACK PANEL: 1.0M WIDE X 5.5M HIGH [3.3' X 18.0']
SANDWICH CONSTRUCTION: STEEL 3mm [1/8" (11Ga.)] - LEAD 13mm[1/2"] - STEEL 6mm[1/4"]
STRUCTURE: 3" X 3" X 1/4" STEEL ANGLE, ALL AROUND
WEIGHT: 3030LB

STANDARD ROOF PANEL: 1.0M WIDE X 3.5M LONG [3.3' X 11.5']
SANDWICH CONSTRUCTION: STEEL 3mm [1/8" (11Ga.)] - LEAD 6mm[1/4"] - STEEL 6mm[1/4"]
STRUCTURE: MC 6 X 16.3 STEEL CHANNEL, ALL AROUND
WEIGHT:2000LB

STANDARD DOOR PANEL: 1.0M WIDE X 2.5M HIGH [3.3' X 8']
SANDWICH CONSTRUCTION: STEEL 3mm [1/8" (11Ga.)] - LEAD 10mm[3/8"] - STEEL 6mm[1/4"]
STRUCTURE: 2" x 2" x 1/8" STEEL ANGLE, ALL AROUND
WEIGHT:1123LB

LABYRINTH PANELS: UTILITIES, CABLES, VENTILATION, OZONE

UTILITIES: CHILLED WATER 5° ± 0.8°C [41° ± 1.5° F]
COMPRESSED AIR 90psi
ELECTRICAL POWER 30kVA 120/208V

ACCESS STATION CRANE WITH MANUAL HOIST:
SPAN 3.5 [11.5'] X RUNWAY LENGTH 7.5M [24.6'] X CLEAR HEIGHT 5.5M [18.0']
CAPACITY: 1000kg [1 TON]

ILLUMINATION: FLUORESCENT - OFFICE RATED: 100 FOOT CANDLE.

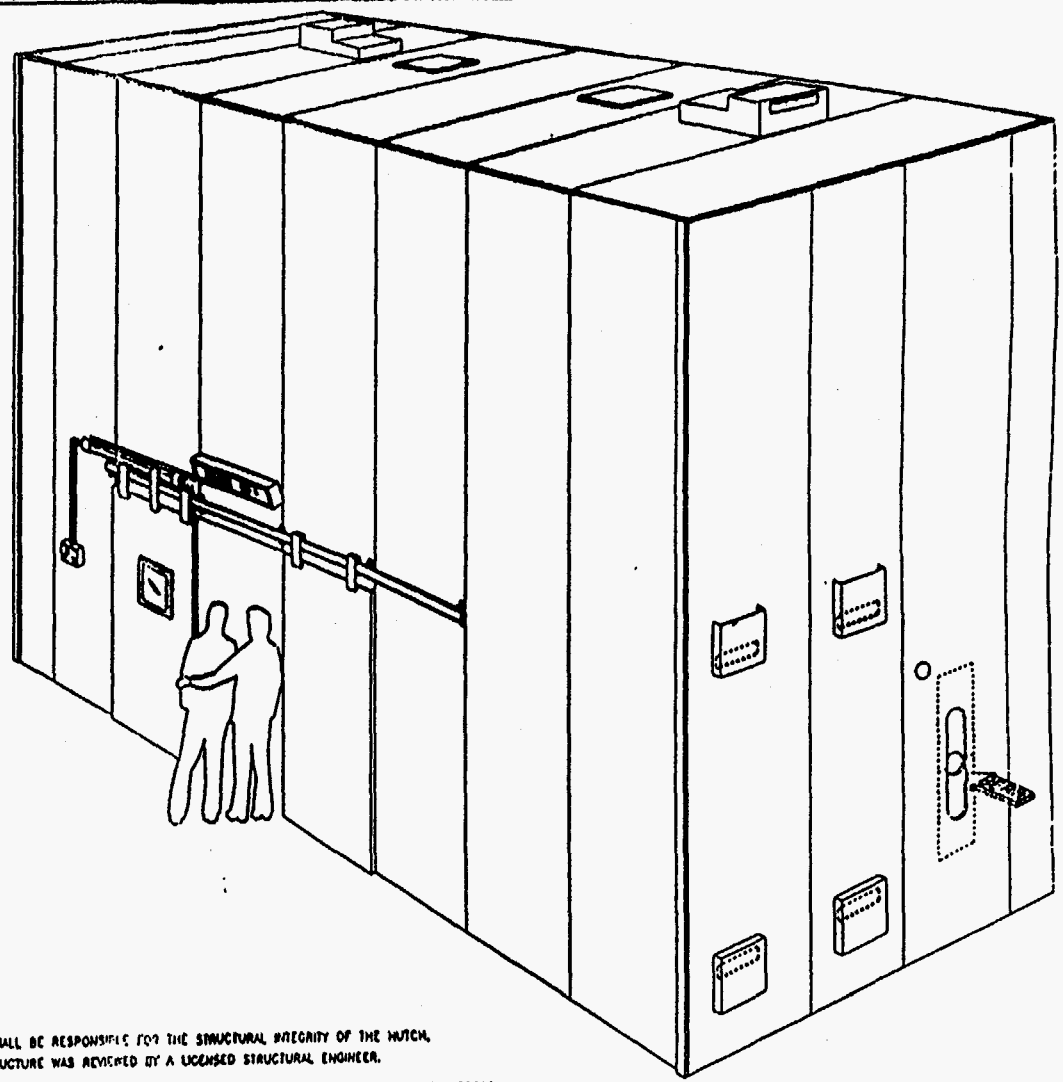

NOTES:

1- THE HUTCH MANUFACTURER SHALL BE RESPONSIBLE FOR THE STRUCTURAL INTEGRITY OF THE HUTCH, AND SHALL CERTIFY THAT THE STRUCTURE WAS REVIEWED BY A LICENSED STRUCTURAL ENGINEER.

STRUCTURES AND THEIR ELEMENTS SHALL BE BUILT FOLLOWING DOE 6430 AS REFERRED IN TECHNICAL SPECS. DESIGN LOAD SHALL INCLUDE LOADS THAT CAN OCCUR DURING CONSTRUCTION. DEAD LOADS SHALL INCLUDE THE USE OF THE INTERIOR UNISTRUT FOR SHELVES ONE FOOT WIDE SUPPORTING LOADS OF 200 LBS.

2- LEAD THICKNESS IS SPECIFIED BY ARGONNE. THE MANUFACTURER SHALL BE RESPONSIBLE FOR PROVIDING A RADIATION LEAK PROVED HUTCH.

LEAD LINED PANELS SHALL BE CONSTRUCTED FROM SINGLE UNPIERCED SHEET, FREE OF OXIDE INCLUSIONS, FISSURES, VOIDS AND ALL OTHER DETRIMENTAL DEFECTS. MATERIAL SHALL BE LEAD GRADE 'C' TO COMPLY WITH FEDERAL SPECIFICATION -QQL201. HUTCH STEEL MEET ALL APPLICABLE RADIATION GUIDE LINES: REFERRED IN TECHNICAL SPECS.

PARTS LIST

A18737

ARGONNE NATIONAL LABORATORY

ADVANCED PHOTON SOURCE
ASD XBES 3-G-C
MONOCHROMATIC BEAM
EXPERIMENTAL STATION ASSY
(PERSPECTIVE & SPECS)

D

PA1050303-610200-XC

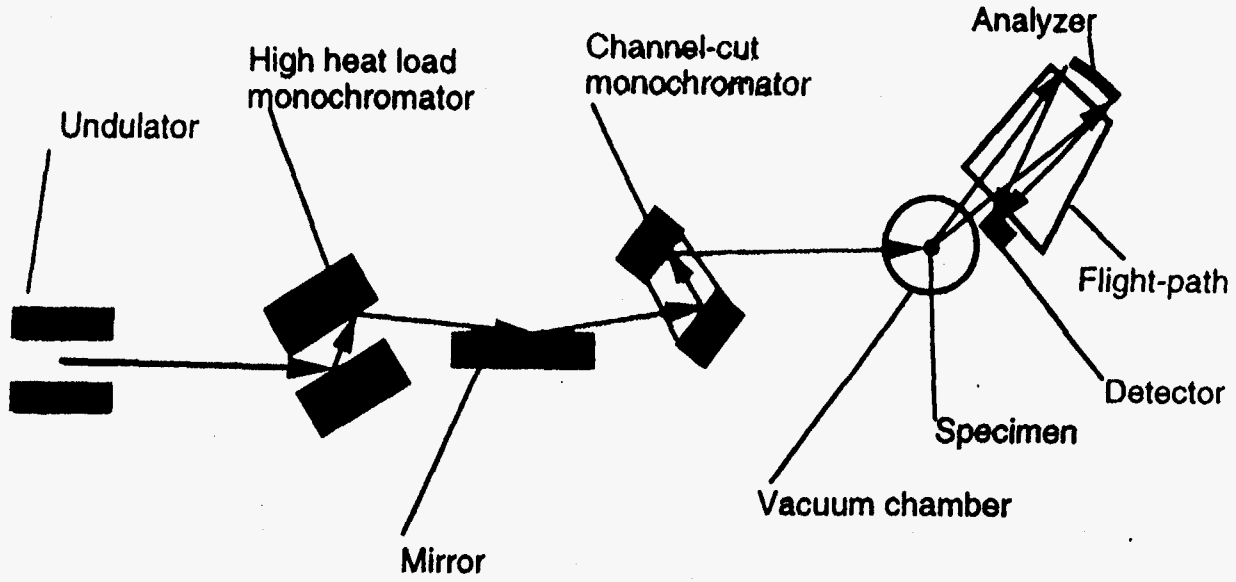

100 MILLI ELECTRON VOLT RESOLUTION INELASTIC SCATTERING SCHEMA

Performance of spherically focusing Ge(444) backscattering analyzers for inelastic x-ray scattering

A. T. Macrander, V. I. Kushnir, and R. C. Blasdell
Experimental Facilities Division, Advanced Photon Source, Argonne National Laboratory, Argonne, Illinois 60439

(Presented on 18 July 1994)

A spectrometer designed for use as an undulator source and having targeted resolutions of 0.01 eV in one mode of use and 0.2 eV in another will operate at the APS. We report here on analyzers that we have constructed for use on this spectrometer for 0.2 eV resolution. We have tested them at NSLS beamline X21 using focused wiggler radiation and at the Cornell high energy synchrotron source (CHESS) using radiation from the CHESS-ANL undulator. Analyzers were constructed by gluing and pressing 90-mm-diam. (111) oriented Ge wafers into concave glass forms having a radius near 1 m. An overall inelastic scattering resolution of 0.3 eV using the (444) reflection was demonstrated at CHESS. Recent results at X21 revealed a useful diameter of 74 mm at an 87° Bragg angle.

I. INTRODUCTION

Since the early 1980's, inelastic x-ray scattering (IXS) has been considered both a desirable and achievable investigative tool with which to attack some of the fundamental problems in condensed matter physics.[1–4] Unlike inelastic neutron scattering, IXS is almost completely unhampered by the kinematic constraints arising from conservation of energy and momentum during the scattering process, and, unlike inelastic electron scattering, x rays penetrate the bulk sufficiently to rule out anomalies due to surface properties. However, cross sections for IXS are extremely small (e.g., 10^{-27} cm^2/eV for the double differential cross section of the plasmon in aluminum[5]) which implies that synchrotron radiation sources should be employed to obtain useful data. With the advent of the APS,[6] which is a third-generation synchrotron source, we expect that sufficiently great incident photon fluxes can be delivered and that spectra of inelastically scattered photons with reasonably good statistics for a wide range of samples can be obtained in scans lasting several hours.

The beamline optical layout will consist of a high-heat-load monochromator followed by a high-resolution monochromator. The diffuse scattering from a sample will be collected by a spherically focusing crystal analyzer.

II. BACKSCATTERING

Backscattering for the analyzer is a propitious geometry because (1) angular Darwin widths become very large, and (2) the derivative of the energy with respect to angle in Bragg's law goes to zero.[7] The consequence of (1) is that the angular acceptance of analyzers increases, and the consequence of (2) is that the resolution becomes less dependent on angular divergence. Because of absorption in the sample, it is favorable to work at as high an energy as possible. Backscattering from silicon at higher energies occurs from high-order reflections [e.g., (777)], which leads to resolutions of several meV. A spectrometer with a 3-m-long two-theta arm designed to employ high-order reflections from a silicon analyzer is under construction on sector 3 of the Synchrotron Radiation Instrumentation (SRI) Collaborative Access Team (CAT) at the APS. A resolution of several meV is useful for the study of phonons. However, it is not needed for the study of electronic excitations and results in an unnecessary bandpass collection penalty in that case.

III. Ge(444) ANALYZER

We have achieved a coarse energy resolution of several hundred meV by using a lower-order reflection [i.e., (444)] from an analyzer made of Ge with a focusing distance of 1 m. At this radius, neither the intrinsic energy width nor the efficiency of a bent Ge wafer is significantly reduced compared to the unbent case. This is demonstrated in Fig. 1 which is the result of a dynamical diffraction simulation.[8] A calculated analyzer resolution of 94 meV FWHM was obtained. Just as in the unbent case, the Darwin width in energy is almost independent of Bragg angle near backscattering.

The most successful procedure we have found to construct an analyzer is (1) first prepare a two-component epoxy mixture by pumping the air out of the mixture in a bell jar,

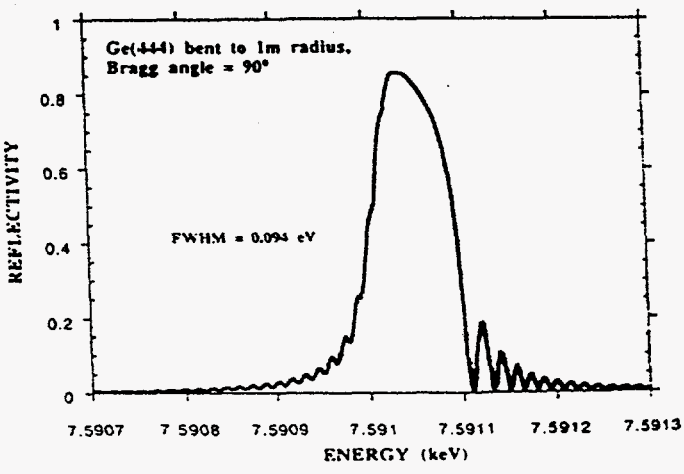

FIG. 1. Reflectivity as calculated using a dynamical matrix simulation method.

 0034-6748/95/66(2)/1546/3/$6.00

7
8
9
10
11
mm
10
20
30
40
50
60
70
80
90
100
110
120

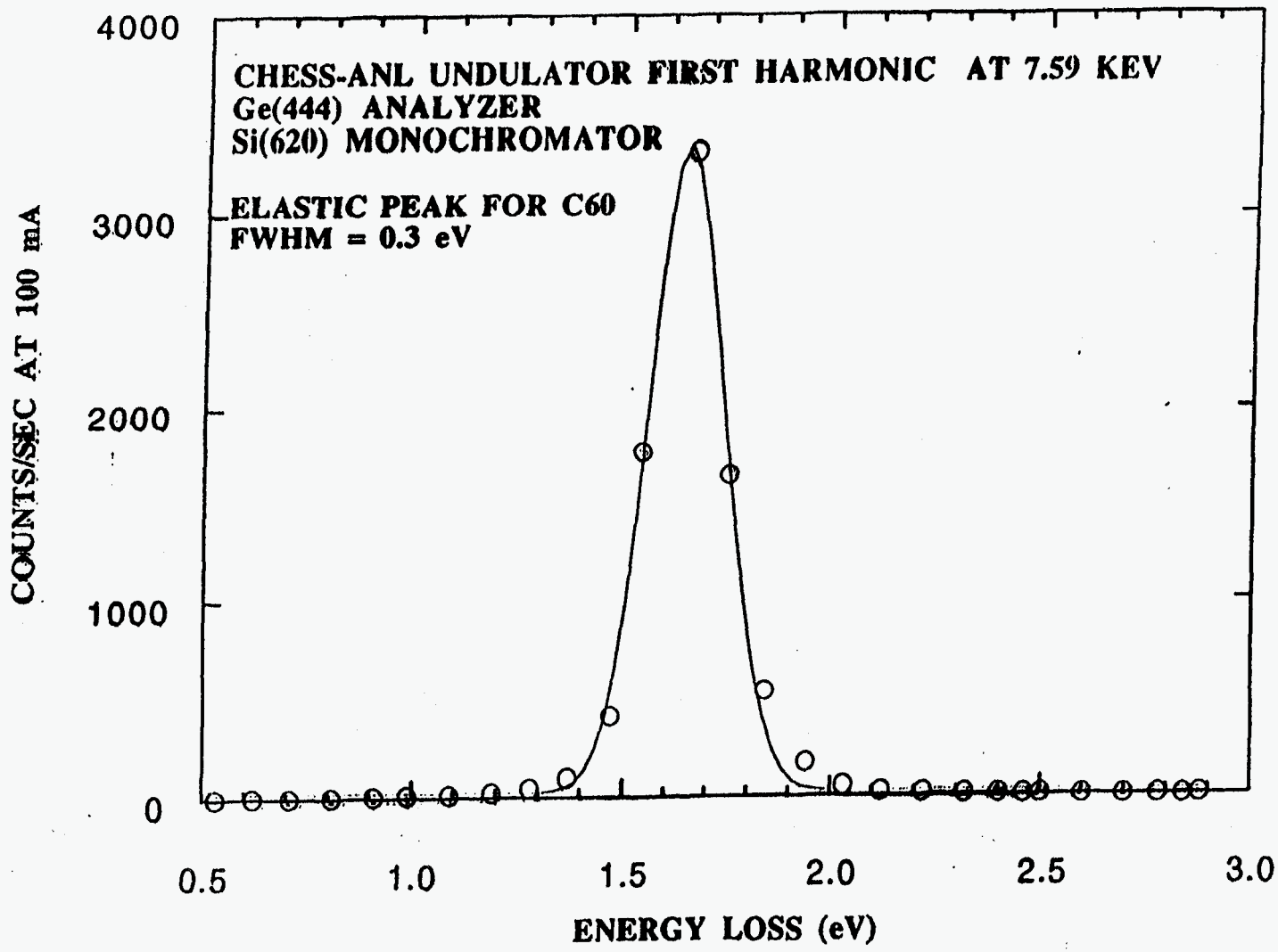
CHESS-ANL UNDULATOR FIRST HARMONIC AT 7.59 KEV
Ge(444) ANALYZER
Si(620) MONOCHROMATOR
ELASTIC PEAK FOR C60
FWHM = 0.3 eV
COUNTS/SEC AT 100 mA
4000
3000
2000
1000
0
0.5
1.0
1.5
2.0
2.5
3.0
ENERGY LOSS (eV)

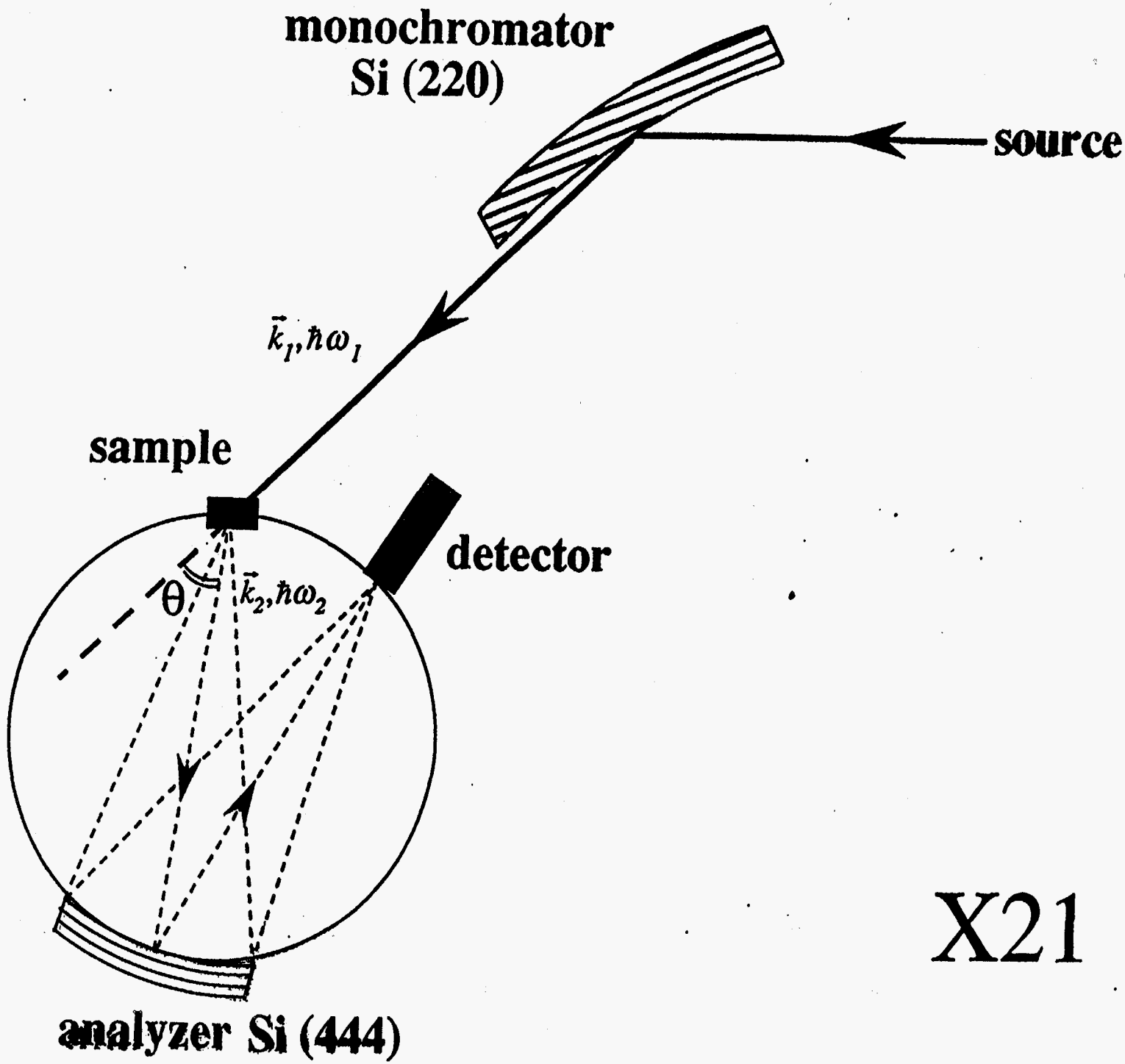
monochromator
Si (220)
source
$\vec{k}_1, \hbar\omega_1$
sample
detector
θ
$\vec{k}_2, \hbar\omega_2$
analyzer Si (444)

X21

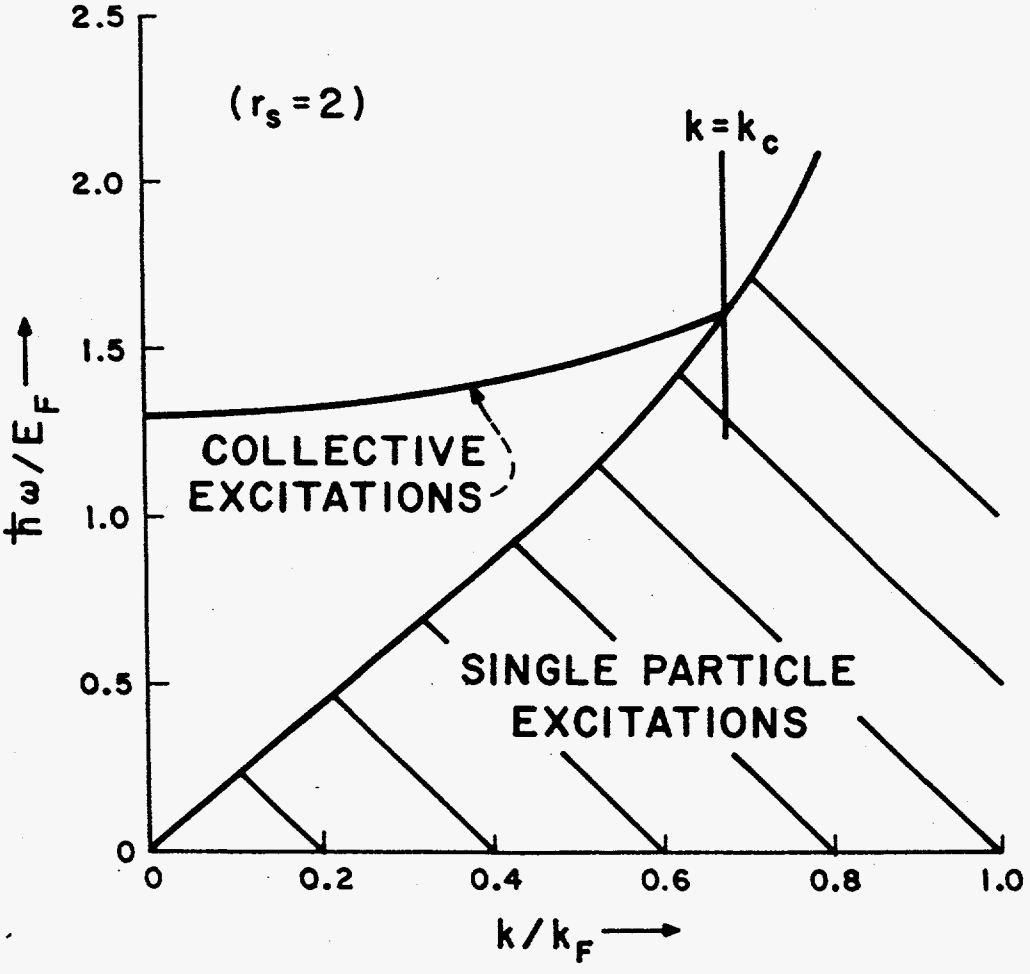

FIG. IV-4. ω–k relationships for excitations of a degenerate electron gas.

P.M. Platzman and P.A Wolf, "Waves and Interactions in Solid State Plasmas", in Supplement 13 of *Solid State Physics*, ed. H. Ehrenreich , F. Seitz, and D. Turnbull, Academic Press, 1973.

Inelastic x-ray scattering from TiC and Ti single crystals

A. T. Macrander
Advanced Photon Source, Argonne National Laboratory, Argonne, Illinois 60439

P. A. Montano
Materials Science Division, Argonne National Laboratory, Argonne, Illinois 60439
and Department of Physics, University of Illinois at Chicago, Chicago, Illinois 60680

D. L. Price
Department of Physics, University of Memphis, Memphis, Tennessee 38152

V. I. Kushnir and R. C. Blasdell
Advanced Photon Source, Argonne National Laboratory, Argonne, Illinois 60439

C. C. Kao
National Synchrotron Light Source, Brookhaven National Laboratory, Upton, New York 11973

B. R. Cooper
Department of Physics, West Virginia University, Morgantown, West Virginia 26506
(Received 29 November 1995)

Inelastic x-ray scattering spectra were measured with incident x rays having an energy near 8 keV for a range of momentum transfers q extending from 0.70 to 2.0 Å $^{-1}$. We find spectral features corresponding to valence electron excitations, as well as Raman scattering corresponding to excitation from the $3p$ core states to the $3d$ valence states of Ti. The spectral features corresponding to valence electron excitations lie in the regime conventionally interpreted as a bulk plasmon together with intraband and interband transitions. We compare our data for TiC at $q = 1.05$ Å $^{-1}$ with calculations for the dynamical dielectric constant $\varepsilon(q,\omega)$ based on local-density theory. The agreement between the data and calculations permits us to interpret certain features in the spectra as arising from band transitions out of the strongly hybridized C $2p$–Ti $3d$ band. The energy loss position of the Raman scattering peak is independent of momentum transfer for both TiC and Ti and lies at 48 eV for Ti. This value is above the highest-lying x-ray ultraviolet absorption resonance for atomic Ti at 43.5 eV. This shift in the data to higher energy transfer is consistent with electron energy loss spectra and photoemission results reported in the literature and indicates that important physical processes are not encompassed within existing theoretical approaches to x-ray Raman scattering. [S0163-1829(96)03425-X]

PACS number(s): 78.70.Ck, 78.30.Hv, 78.30.−j

I. INTRODUCTION

Inelastic x-ray scattering (IXS) spectra are a source of information on the dynamics of electronic excitations.[1] With a bandpass ranging from 0.1 to 1 eV, IXS can be used to study both valence band and conduction band excitations as well as plasmons. In addition, x-ray Raman scattering involving excitations out of core states can be studied. Because the intrinsic scattering cross section for x rays is ten orders of magnitude smaller than for electrons, the bulk properties of samples can be studied without interference from surface effects as occurs in the case of electron energy loss spectroscopy (EELS). Furthermore, hard x rays do not require the use of ultrahigh-vacuum conditions.

Because scattering rates are significantly reduced for heavily absorbing samples, IXS studies have been limited to materials with low atomic number. Be,[2,3] Li,[4,5] and Al,[6,7] as well as graphite[5] and C_{60},[8] have been studied. A detailed study of Si has also recently appeared.[9] In this work we have extended this list to include the elemental transition metal Ti, as well as the binary material TiC.

The rare combination of strong bonding and metallic conductivity has attracted theoretical attention to the electronic structure of TiC. Furthermore, the simple rocksalt crystal structure has facilitated the calculation of the full dielectric constant $\varepsilon(q,\omega)$ using a full-potential linearized combination of muffin-tin orbitals (LMTO).[10] Here $\hbar\omega$ and $\hbar q$ are the energy and momentum lost by the x-ray photon upon scattering. A sum over the Brillouin zone is required to obtain the wave-vector- and frequency-dependent dielectric constant, and obtaining this sum is an involved procedure.[11]

Broadly speaking, we can divide the IXS processes that involve electronic excitations into two regimes of ω. Plasmons and valence band excitations occur at lower values, and inner shell excitations occur at higher values in the Raman regime. We report here spectral bands for both materials that fall into the plasmon and band excitations regime and are well accounted for by these excitations. In addition, there is for both materials a higher-lying spectral band to which existing theoretical approaches to Raman scattering do not lend an explanation.

II. EXPERIMENTAL DETAILS AND RESULTS

The IXS spectra were measured at beam line X21 at the National Synchrotron Light Source. This beam line has a wiggler as a source and delivers 2×10^{11} photons per second in a bandwidth of about 0.7 eV.[12] Crystal analyzers of increased collection efficiency have recently been constructed and were used for the present studies. These analyzers were Si(444) at 7.9 keV (Ref. 12) and Ge(444) at 7.6 keV.[13] Both of these were operated at Bragg angles in the range 86°–87°. The spectra were obtained by scanning the incident energy with a fixed analyzer setting, i.e., at a fixed collection energy. We used a Ge solid-state detector to record the scattered photons.

We made measurements on single crystals of TiC and Ti. The TiC crystal had a large facet oriented 20° away from [111], and we inclined the crystal by 20° to position the [111] direction along the scattering vector q. The Ti crystal was oriented so that q lay along [00·1], i.e., along the c axis of the hexagonal structure. The raw spectra for TiC and Ti are shown in Figs. 1 and 2, respectively. The data are shown with low ordinate values of each spectrum brought to the zero of the ordinate scale. The data were normalized to the incident beam by using an ion chamber placed in front of the sample.

III. BASIC RELATIONS AND LOCAL-DENSITY-APPROXIMATION CALCULATIONS

Within the first Born approximation, the double differential cross section is related to the dynamical structure factor $S(\mathbf{q},\omega)$ by the well-known relationship[14]

$$\frac{d^2\sigma}{d\omega\,d\Omega}=(\mathbf{e}_1\cdot\mathbf{e}_2)r_0^2\frac{\omega_2}{\omega_1}S(\mathbf{q},\omega), \tag{1}$$

where $\hbar\omega_1$ and $\hbar\omega_2$ are the energies of the incident and scattered photons, respectively, and $\mathbf{e}_1$ and $\mathbf{e}_2$ are their polarization vectors. The Thomson factor e^2/mc^2 is written as r_0, the classical electron radius. The dynamical structure factor is related to the dielectric response function $\varepsilon(\mathbf{q},\omega)$ by the fluctuation-dissipation theorem[15]

$$S(\mathbf{q},\omega)=-\frac{\hbar q^2}{4\pi^2e^2n}\mathrm{Im}\left(\frac{1}{\varepsilon(\mathbf{q},\omega)}\right). \tag{2}$$

Here n is the electron density.

There are two approaches to the calculation of $1/\varepsilon(\mathbf{q},\omega)$ that have been applied to fitting to $S(\mathbf{q},\omega)$ obtained by IXS.[5] The first approach starts with the jellium model, which reduces the effect of the ion cores to that of a uniform positive background. One proceeds by treating the electron-electron interactions within the random-phase-approximation (RPA).[15] In this way the following expression, which is known as Lindhard's longitudinal dielectric function,[16] is obtained:

$$\varepsilon^L(\mathbf{q},\omega)=1-\lim_{\delta\to0}V_q\sum_{\mathbf{p}}\frac{f(E(\mathbf{p}+\mathbf{q}))-f(E(\mathbf{p}))}{E(\mathbf{p}+\mathbf{q})-E(\mathbf{p})-\hbar\omega+i\delta}. \tag{3}$$

Here $E(\mathbf{p})$ and $f(E(\mathbf{p}))$ are the single-particle energy and Fermi occupational factor of the eigenstate having a momentum p, and V_q equals $4\pi e^2/q^2\Omega$, with Ω denoting the volume. Corrections for electron-electron interactions beyond the RPA, i.e., for exchange and correlation, are then incorporated via a local field factor[17] and by the introduction of a finite lifetime of the single-particle states.[18] For small q, the Lindhard dielectric constant has a pole corresponding to a plasmon. Within the RPA there is no decay mechanism for the plasmon as long as energy and momentum conservation

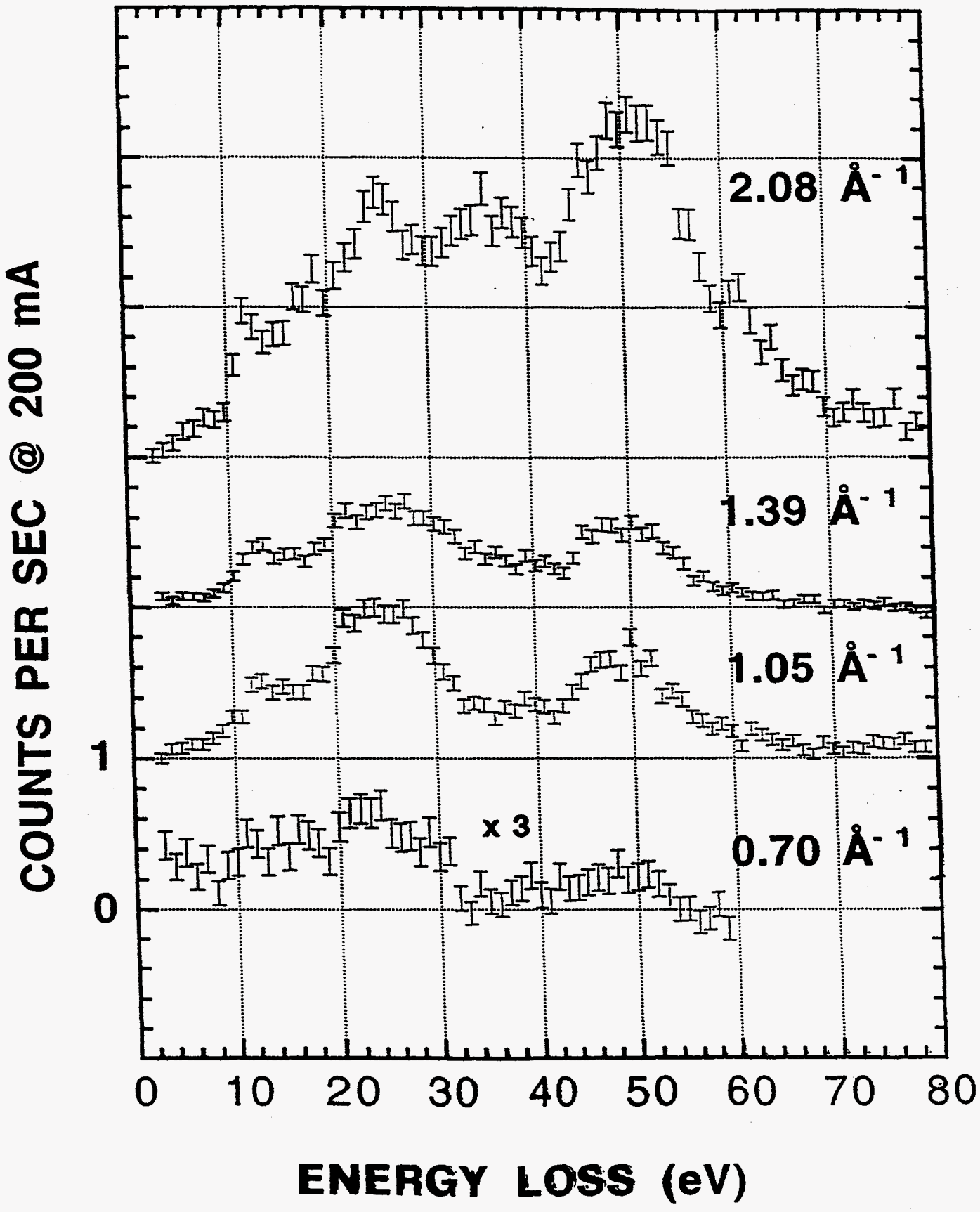
COUNTS PER SEC @ 200 mA
2.08 Å⁻¹
1.39 Å⁻¹
1.05 Å⁻¹
0.70 Å⁻¹
x 3
1
0
0
10
20
30
40
50
60
70
80
ENERGY LOSS (eV)

TABLE I. Free electron values.

	TiC (NaCl)	Ti (hcp)
a, lattice parameter (Å)	4.33	2.95
c, lattice parameter (Å)		4.68
Electrons in unit cell	32	8
n, electron density (Å^{-3})	0.394	0.227
ω_p, plasmon energy (eV)	23.3	17.7
q_c, critical momentum (Å^{-1})	1.09	0.98

do not permit the creation of electron-hole pairs. For q larger than q_c, where q_c is defined as the plasmon momentum consistent with the kinematic constraints imposed on electron-hole formation, the plasmon can decay. Plasmon dispersion within the RPA is given by[19]

$$\omega^2 = \omega_p^2 + \tfrac{3}{5} v_F^2 q^2. \tag{4}$$

Here v_F is the Fermi velocity. Values for n, $\omega_p = \sqrt{4\pi n e^2/m}$, and q_c for TiC and Ti are listed in Table I.

Comparing these to the data, we see that the strong peaks near 24 eV for TiC and near 19 eV for Ti correspond roughly to the expected plasmon energy. Furthermore, of all the q's investigated, the value of 1.05 Å^{-1} is closest to q_c for both TiC and Ti. For values of q larger than q_c, the discrete plasmon excitation couples to the continuum of electron-hole excitations and spectra in this region have been interpreted by including so-called Fano resonances or antiresonances.[9] In addition, the plasmon corresponding to the next reciprocal lattice vector may also be excited.[9] These two phenomena are expected to enter into a complete theoretical description of our data for $q > q_c$.

There are clear peaks in the $S(q,\omega)$ data for TiC taken at $q = 1.05$ Å^{-1} at ~ 12 and ~ 50 eV that are not explained within the framework of the jellium model as we have outlined it, and the next logical step, the incorporation of band structure, is presented below.

We applied the Ehrenreich-Cohen[20] expression for the dielectric function given by

$$\varepsilon(q,\omega) = 1 - \lim_{\delta \to 0} V_q \sum_{r,s,\mathbf{p}} |\langle \Psi_r(\mathbf{p}) | e^{-i\mathbf{q}\cdot\mathbf{r}} | \Psi_s(\mathbf{p}+\mathbf{q}) \rangle|^2 \frac{f(E_s(\mathbf{p}+\mathbf{q})) - f(E_r(\mathbf{p}))}{E_s(\mathbf{p}+\mathbf{q}) - E_r(\mathbf{p}) - \hbar\omega + i\delta}. \tag{5}$$

Here r and s are band structure indices. We note that this is the first diagonal element of a more general dielectric matrix with separate elements for separate reciprocal lattice vectors.[19] Neglect of these other terms corresponds to the neglect of microscopic local field effects, i.e., field effects due to the periodicity of the solid.[5] Equation (5) derives from self-consistent field theory[20] and is equivalent to the RPA.[5] Introduction of exchange, correlation, and lifetime effects is thought to be possible via the same techniques as outlined above for the jellium model,[5] although this is a largely untested hypothesis.

However, we have taken a different approach in which we evaluate Eq. (5) using wave functions and eigenvalues derived from local-density-functional theory.[21] This approach incorporates local exchange via the potential of Ceperley and Alder.[22] Due in part to the simple rock salt structure of TiC, we have been able to obtain the dielectric function for $q = 1.05$ Å^{-1}. The band sums were performed over the one-electron valence and conduction bands in the first Brillouin zone. Results for $\mathrm{Im}(\varepsilon)$, $\mathrm{Re}(\varepsilon)$, and $\mathrm{Im}(1/\varepsilon)$ are shown in Fig. 3. Invoking the fluctuation-dissipation theorem, we compare the calculated values for $\mathrm{Im}(1/\varepsilon)$ to our data in Fig. 4. Here we have convolved the raw calculated results with a Gaussian resolution function having a full width at half maximum (FWHM) of 0.8 eV. This value was measured by us for the FWHM of the elastic peak of a Plexiglas sample. The ordinate scale was obtained by applying the f-sum rule to both our data and the calculations. The f-sum rule is given by

$$\int \omega S(q,\omega)\, d\omega = \frac{\hbar q^2}{2m}. \tag{6}$$

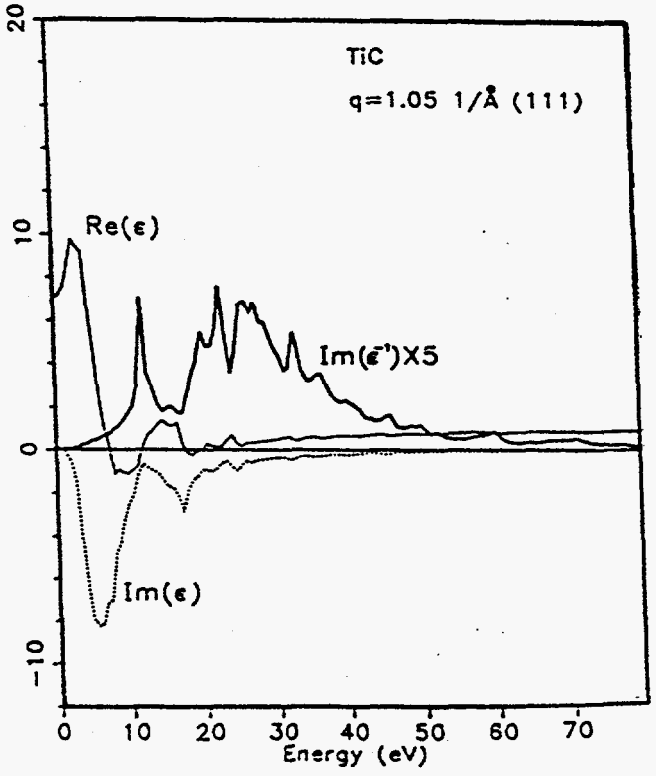

FIG. 3. Calculated values for the real and imaginary parts of the dielectric constant and for $\mathrm{Im}(1/\varepsilon)$ for TiC for $q = 1.05$ Å^{-1} along [111].

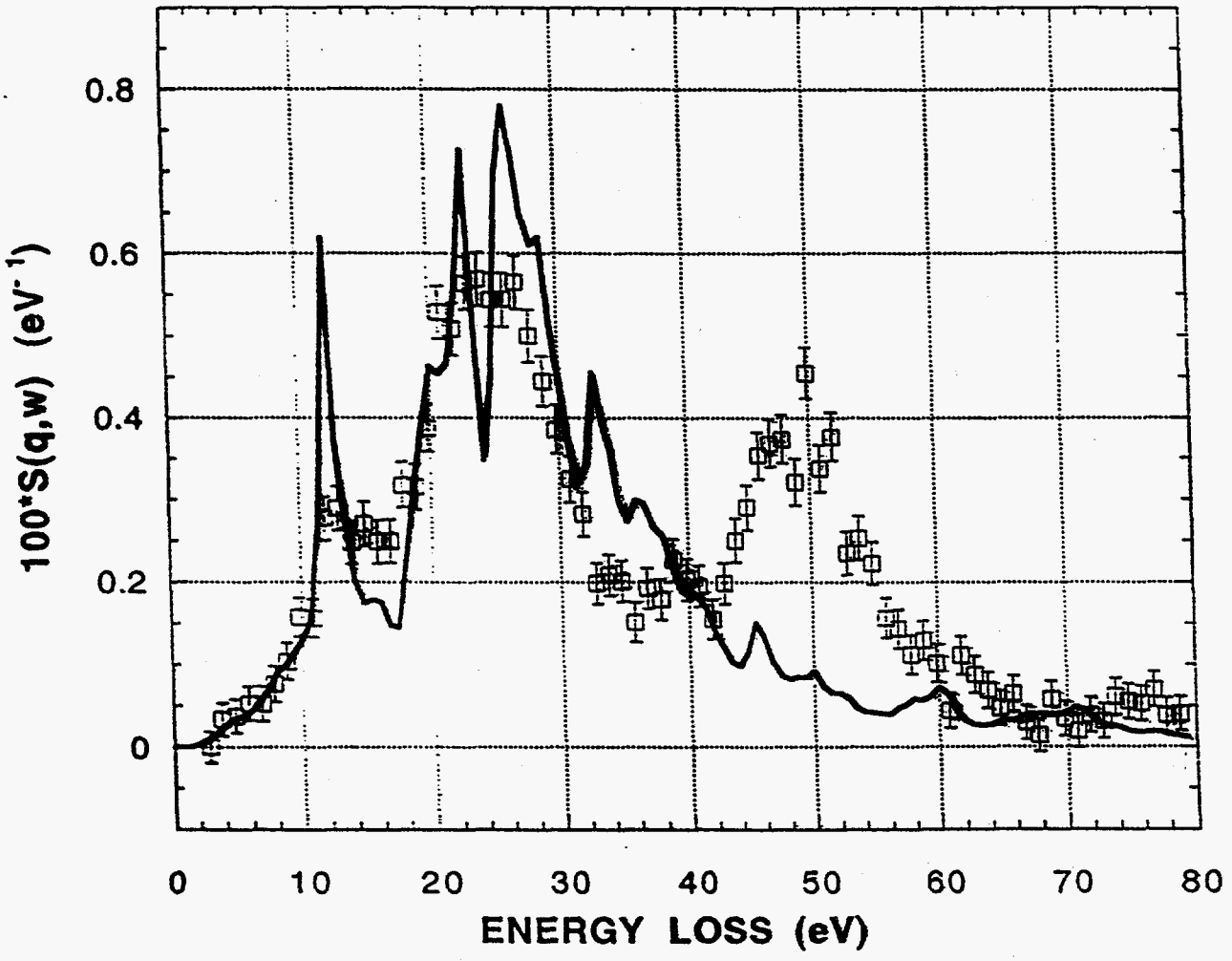
0.8
0.6
0.4
0.2
0
100*S(q,w) (eV-1)
0
10
20
30
40
50
60
70
80
ENERGY LOSS (eV)

ENERGY (eV)

33.4 ± 0.1
36.6 ± 0.2
38.9 ± 0.1
41.2 ± 0.1
43.5 ± 0.2

from: B.Sonntag and P.Zimmermann, Rep. Prog. Phys. 55, 911 (1992), Table 3.

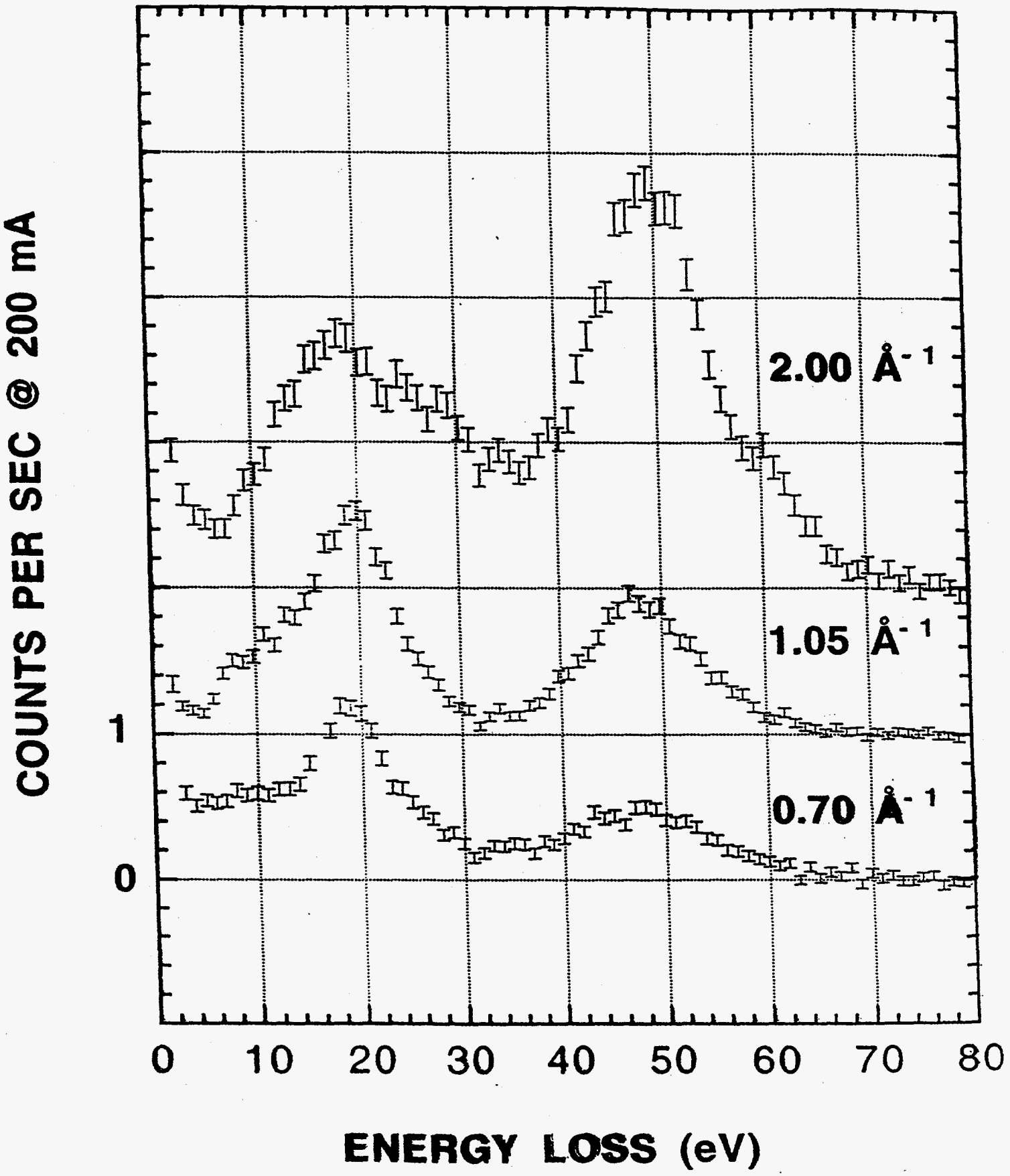
COUNTS PER SEC @ 200 mA
2.00 Å⁻¹
1.05 Å⁻¹
0.70 Å⁻¹
1
0
0
10
20
30
40
50
60
70
80
ENERGY LOSS (eV)

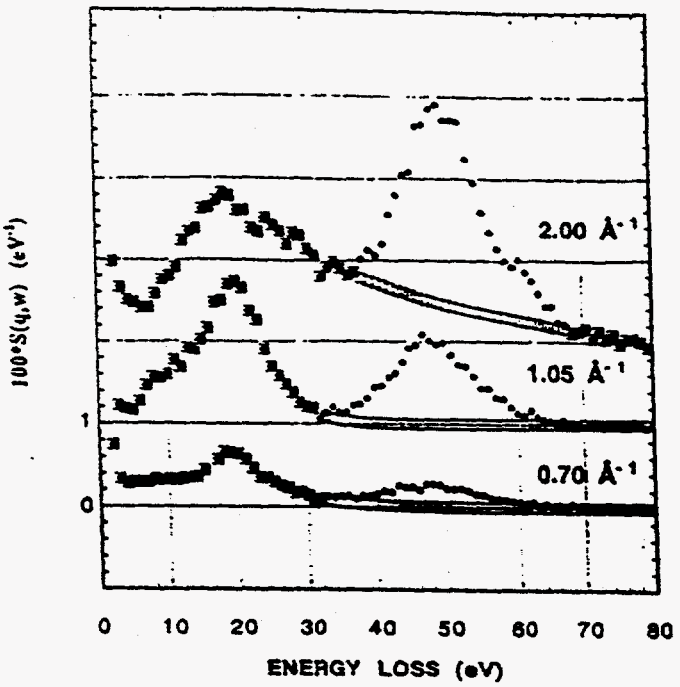

FIG. 9. $S(q,\omega)$ for Ti. The ordinate scale was obtained from the IXS data by applying the f-sum rule to the points shown as squares. The Raman contribution to the spectrum is the difference between the data shown as solid circles and squares.

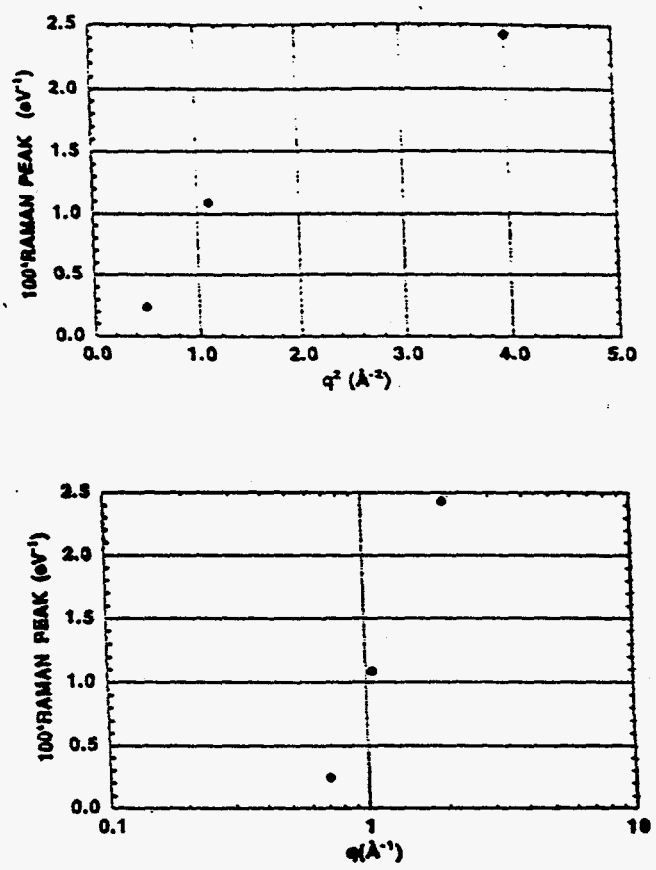

FIG. 10. Peak Raman contribution to $S(q,\omega)$ plotted vs q^2 in the top part of the figure and vs $\ln(q)$ in the bottom part.

Å^{-1} centered near 35 eV, a value between the lowest two absorption resonances listed in Table II. We surmise that this peak corresponds to the actual onset of the $3p$ to $3d$ absorption edge, but this conclusion must await further theoretical developments.

A theory of x-ray Raman scattering has been formulated based on a one-electron picture and has yielded the Golden rule relationship[34–36]

$$S_R(\mathbf{q},\omega)=\sum_{\mathbf{p}} |\langle \mathbf{p}|e^{i\mathbf{q}\cdot\mathbf{r}}|0\rangle|^2 \delta(E(\mathbf{p})-E(0)-\hbar\omega). \quad (9)$$

When analyzed within the dipole approximation and when applied to an isotropic solid, one obtains

$$S_R(\mathbf{q},\omega)=\frac{cq^2}{4\pi^2 e\omega}\sigma(\omega), \quad (10)$$

where $\sigma(\omega)$ is the soft x-ray absorption cross section. If Eq. (10) applies, the Raman spectrum should have essentially the same shape as the absorption spectrum.[36]

Our data do not reveal a clear absorption edge followed by a plateau as was observed for x-ray Raman spectra of Li.[5] This qualitative difference for our data casts suspicion on the approximations made in deriving Eq. (10). An analysis of the q dependence of our Ti data confirms the inadequacy of Eq. (10) in describing our Raman results. We applied the f-sum rule, which is derived from a particle conservation condition,[15] to place the ordinate on an absolute scale for $S(q,\omega)$ of the valence electron excitations. Following Nagasawa, Mourikis, and Schulke,[36] the sum rule was applied after subtracting the Raman portion of the spectrum as shown in Fig. 9. The peak amplitude above the tail of the valence electron excitations is plotted as a function of q^2 in the upper panel of Fig. 10. We find that the q^2 dependence of Eq. (10) does not hold. We find instead a logarithmic dependence as shown in the lower panel of Fig. 10. Only terms that are higher order in q (e.g., quadrupole) are expected based on Eq. (9), and consequently we conclude that the above theoretical description does not apply to our experimental results.

V. SUMMARY AND CONCLUSIONS

Inelastic x-ray scattering spectra for TiC and Ti are reported. The spectra are informative not only about valence excitations, but also about high-energy loss excitations out of the $3p$ core states of Ti. The valence excitations are compared to results of calculations made using local-density functional theory, and we find that we can relate certain spectral features to band transitions. The q dependence of the core excitation part of the spectrum disagrees with a one-electron theoretical description applied to an isotropic solid

ACKNOWLEDGMENTS

We are grateful to D. M. Mills, G. K. Shenoy, D. F. Moncton, J. B. Hastings, and D. B. McWhan for encouragement in this project. We acknowledge helpful discussions with J. L. Dehmer and P. M. Platzman. We would like

SUMMARY

IXS with 10 meV resolution for phonons
IXS with 200 meV resolution for electronic excitations